



RESEARCH ARTICLE | APRIL 17 2024

Relativistic R-matrix calculations for the photoionization of W^{61+} ions

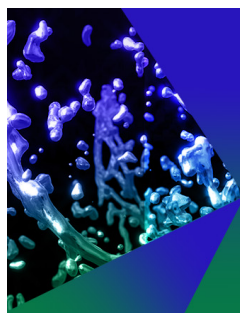
Special Collection: [Proceedings of PLASMA 2023 - International Conference on Research and Applications of Plasmas](#)

Z. W. Wu ; J. Q. Wang; Y. Li; Y. H. An; S. Fritzsche 



Phys. Plasmas 31, 043301 (2024)

<https://doi.org/10.1063/5.0201766>



Physics of Plasmas

Publish open access for **free**

[Learn More](#)

Relativistic R-matrix calculations for the photoionization of W^{61+} ions

Cite as: Phys. Plasmas **31**, 043301 (2024); doi: [10.1063/5.0201766](https://doi.org/10.1063/5.0201766)

Submitted: 31 January 2024 · Accepted: 2 April 2024 ·

Published Online: 17 April 2024



View Online



Export Citation



CrossMark

Z. W. Wu,^{1,2,3,a)} J. Q. Wang,¹ Y. Li,¹ Y. H. An,¹ and S. Fritzsche^{2,3,4}

AFFILIATIONS

¹Key Laboratory of Atomic and Molecular Physics & Functional Materials of Gansu Province, College of Physics and Electronic Engineering, Northwest Normal University, Lanzhou 730070, People's Republic of China

²Helmholtz-Institut Jena, Fröbelstieg 3, D-07743 Jena, Germany

³CSI Helmholtzzentrum für Schwerionenforschung GmbH, Planckstrasse 1, D-64291 Darmstadt, Germany

⁴Theoretisch-Physikalisches Institut, Friedrich-Schiller-Universität Jena, Max-Wien-Platz 1, D-07743 Jena, Germany

Note: This paper is part of the Special Topic, Proceedings of PLASMA 2023 - International Conference on Research and Applications of Plasmas.

^{a)} Author to whom correspondence should be addressed: zhongwen.wu@nwnu.edu.cn

ABSTRACT

Direct and resonant photoionization of Al-like W^{61+} ions from their ground state $1s^2 2s^2 2p^6 3s^2 3p^2 P_{1/2}$ and four lowly excited states $1s^2 2s^2 2p^6 3s^2 3p^2 P_{3/2}$, $1s^2 2s^2 2p^6 3s 3p^2 P_{1/2,3/2}$, and $1s^2 2s^2 2p^6 3s 3p^2 D_{5/2}$ is studied by using the multiconfigurational Dirac-Fock method and the relativistic R-matrix method. Emphasis is placed upon exploring direct and resonant ionization limits and also upon identifying possible resonance channels of W^{61+} ions. To do so, the photoionization cross sections are calculated with the use of the Dirac Atomic R-matrix Code. For the ground-state photoionization, the direct and resonant ionization limits are obtained, and the identified resonance peaks are found to be associated with the resonances $1s^2 2s^2 2p^6 3s 3p^2 P_{1/2}$ and $1s^2 2s^2 2p^6 3p 3p^2 P_{1/2}$ ($l, l' = p, d$) at a level of fine-structure energy level or configuration. For the excited-state photoionization, however, although the respective direct ionization limits are obtained, the resonant ionization limits and resonance peaks are hardly distinguishable due to much more densely spaced resonance peaks and complex resonance structure. It is expected that the present work could fill the vacancy of studies on the photoionization of W^{61+} ions and be helpful to the diagnosis and simulation of the thermonuclear fusion plasmas together with other available photoionization data of tungsten ions with other charge states.

© 2024 Author(s). All article content, except where otherwise noted, is licensed under a Creative Commons Attribution (CC BY) license (<https://creativecommons.org/licenses/by/4.0/>). <https://doi.org/10.1063/5.0201766>

I. INTRODUCTION

The interaction of light with matter through photoionization of atoms and ions is a significant process in nature. This process occurs often in a variety of laboratory plasmas^{1–3} and astrophysical plasmas^{4–8} existing in the vicinity of intensive radiation sources, such as binary stars, accretion disks, and magnetized neutron stars. A systematic study of atomic and ionic photoionization is particularly significant in the fields of atomic physics, plasma physics, and astrophysics. For example, photoionization studies can be used to study electronic structure of ions, characterization of ionization thresholds, autoionizing resonances, isotope shifts, and fine-structure effects.⁹ As the interaction of photons with atoms or ions is a fundamental atomic process in a variety of plasma environments,¹⁰ laboratory investigations of photoabsorption and photoionization are, therefore, important in the context of a wide range of modeling and applications.¹¹ Moreover, the process

also plays a key role in high-temperature environment of controlled thermonuclear fusion devices.¹²

During the past few decades, great emphasis has been laid upon photoionization studies of atoms and ions.¹³ In particular, photoionization data are strongly needed in many fields, such as astrophysical modeling for opacities, modeling of laboratory plasmas, astrophysical plasmas and fusion plasmas, spectral analysis, ionization balance, and recombination cascade matrix,¹⁴ and it is also a potential tool for exploring the role of intermediate multiply excited states in photon-ion interactions by performing photoionization measurements along with detailed theoretical calculations.¹⁵ Actually, a number of theories have been developed for detailed and accurate study of the photoionization process of atoms and ions. The widely known theoretical approaches include the fully relativistic distorted-wave method,¹⁶ the multiconfigurational Hartree-Fock method,¹⁷ the quantum defect theory,¹⁸

the multi-configurational Dirac–Fock (MCDF) method,¹⁹ and the R-matrix method.²⁰ By using these methods, atomic and ionic photoionization processes have been extensively studied for light elements.^{21–25} Among these studies, the effects of an electronic structure of atoms and ions, the electron correlation, the hyperfine interaction as well as the quantum many-body and relativistic effects on the photoionization processes have been also explored.²⁴ On the basis of these studies along with other relevant research, several important databases were established, such as the opacity project^{26,27} and the iron project.²⁸

Tungsten has become the focus of attention on fusion research, being considered as the main candidate for the cover of the plasma-facing component in next-generation fusion devices like the International Thermonuclear Experimental Reactor Tokamak (ITER). This is due to the fact that tungsten has excellent physical and chemical properties, such as high sputtering threshold energy, low sputtering yield, high re-deposition efficiency, and low tritium retention.²⁹ However, tungsten impurity ions are produced due to the interaction between the edge plasma and the cover materials. These ions may be transported to the fusion core plasmas and further be ionized to produce even highly charged tungsten ions. The resulting highly charged tungsten ions could cause a large radiation loss by emitting high-energy photons, which leads to plasma disruption when the relative concentration of tungsten ion impurities in the core plasma is higher than about 10^{-5} magnitude.²⁹ Monitoring and controlling the flux of these highly charged tungsten impurity ions is important to retain the fusion.³⁰ To monitor and control the tungsten impurity ion flux produced by the interaction between the edge plasma and the cover materials, the atomic data of tungsten ions are indispensable.³¹ Furthermore, in the existing thermonuclear fusion, facilities with tungsten as the facing material tungsten ions with medium and high charge states can be generated, while in the ITER, the highest charge state is expected to be higher than W^{64+} and the electron temperature of the corresponding fusion plasmas is higher than 30 keV.^{32,33} At such high electron temperatures, high-energy x-ray radiations with several tens of kiloelectron volt exist extensively in the fusion plasmas, which makes the photoionization of highly charged tungsten ions possible. As one of the dominant atomic processes for altering the charge state of ions, photoionization of tungsten and its ions plays a very important role in the ionization balance and energy transfer of fusion plasmas. The analysis of photoionization of tungsten ions furnishes valuable information about the role of tungsten atoms and ions in a plasma.³⁴ Therefore, a great number of theoretical and experimental studies have been carried out for the direct and resonant photoionization of tungsten and its ions with various charge states.

For example, Boyle *et al.*³⁵ calculated photoionization cross sections of atomic tungsten for photon energies ranging from the ionization threshold of tungsten to 150 eV by using the many-body perturbation theory. Sladeczek *et al.* measured the first photon yield spectra of W^+ and W^{2+} ions in the range of 30–60 eV using atomic tungsten beam and monochromatic synchrotron radiation excitation method.³⁶ Ballance and McLaughlin performed large-scale theoretical calculations of total photoionization of the 4f, 5s, 5p, and 6s orbitals of neutral tungsten atoms using the Dirac–Coulomb R-matrix approximation.^{37,38} Photoionization cross sections of W^+-W^{5+} ions were studied both experimentally and theoretically by Müller *et al.*^{39–44} The experiments were carried out at the photon-ion merged-beam facility of the Berkeley Advanced Light Source, and the theoretical results

were obtained by the Dirac–Coulomb R-matrix method. In addition to neutral tungsten atoms and lowly charged tungsten ions, the photoionization of highly charged tungsten ions has been also studied extensively. Trzhaskovskaya and Nikulin calculated photoionization cross sections for $W^{3+}-W^{13+}$, $W^{14+}-W^{23+}$, $W^{24+}-W^{45+}$, and $W^{47+}-W^{71+}$ ions, which are important to fusion plasma research associated with facilities such as the ITER, ASDEX-U, and Electron Beam Ion Trap.^{45–48} The direct photoionization of W^{63+} and W^{64+} ions was studied using the perturbed dipole method and the Sturmian model by López *et al.*⁴⁹ Khatri *et al.* calculated the photoionization cross sections of Ne-like W^{64+} ions from the ground state $1s^2 2s^2 2p^6 \ ^1S_0$ by using the Dirac–Coulomb R-matrix method under the close-coupling approximation.³⁴ Moreover, we also performed relativistic R-matrix calculations for the photoionization of W^{63+} ions from their ground state $[Ne] 3s^2 S_{1/2}$ and four lowly excited states $[Ne] 3p^2 P_{1/2,3/2}$ and $[Ne] 3d^2 D_{3/2,5/2}$.⁵⁰

Nevertheless, the existing studies of the photoionization of tungsten ions with very high charge states and the relevant photoionization data are still scarce.⁴⁹ In the present work, the resonant photoionization processes from the ground state $[Mg] 3p^2 P_{1/2}$ and the first four excited states $[Mg] 3s^2 3p^2 P_{3/2}$, $[Ne] 3s 3p^2 P_{1/2,3/2}$, and $[Ne] 3s 3p^2 D_{5/2}$ of Al-like W^{61+} ions are studied by using the relativistic Dirac–Coulomb R-matrix method.

This contribution is structured as follows: In Sec. II, the R-matrix method for the study of atomic and ionic photoionization is given briefly. In Sec. III, we discuss the presently obtained results for the photoionization of W^{61+} ions, in particular, the corresponding cross sections and resonance peak structure. Finally, a brief conclusion is summarized in Sec. IV. Atomic units have been used throughout this paper unless stated otherwise.

II. THEORY AND COMPUTATION

Winger and Eisenbud initiated the R-matrix method in 1947 for the study of nuclear reactions.⁵¹ As the development of the R-matrix method, it has been employed nowadays to describe various atomic collision and photoionization processes. A major breakthrough is the release of the Dirac Atomic R-matrix Code (DARC) in 2004 based on the relativistic R-matrix method,⁵² which facilitated the study of collision and photoionization processes of highly charged ions, which can be strongly affected by the relativistic effects.

Since the relativistic R-matrix method has been described in great detail by Norrington,⁵² in this paper we just describe briefly the main elements of the method. In the R-matrix method, the Dirac–Coulomb Hamiltonian of a $(N+1)$ -electron system is expressed as^{52,53}

$$H^{N+1} = \sum_{i=1}^{N+1} \left[\left(-i\alpha \cdot \nabla_i + (\beta - 1)c^2 - \frac{Z}{r_i} \right) + \sum_{j=i+1}^{N+1} \frac{1}{|\mathbf{r}_i - \mathbf{r}_j|} \right]. \quad (1)$$

Here, α and β represent the Dirac matrices constructed in terms of the Pauli matrices and a 2×2 identity matrix. The four terms in the Hamiltonian represent the single-electron momentum term, the single-electron mass term, the Coulomb interaction between the (bound) electron and the nucleus with nuclear charge Z , and the Coulomb repulsion between the i th and j th electrons. The angular variables of the corresponding Hamiltonian matrix elements are calculated by using the Racah algebra, while the radial part is calculated numerically.

In the close-coupling approximation, the wavefunction of the $(N+1)$ -electron system in the internal region can be formally expressed as^{52,53}

$$\Psi_k^{N+1} = \sum_{ij} c_{ijk} \hat{A} [\Phi_i^N, u_{ij}]^{J\pi} + \sum_q d_{qk} \theta_q^{N+1}. \quad (2)$$

In this expression, $\hat{A} [\Phi_i^N, u_{ij}]^{J\pi}$ denotes the coupled wavefunction of the $(N+1)$ -electron system with total angular momentum J and parity π , which is approximated by using the N -electron target-state wavefunction $\Phi_i^N = |J_i^t \pi_i^t\rangle$ and the basis functions $u_{ij} = |\varepsilon \kappa m\rangle$ of the continuum orbitals with kinetic energy ε and relativistic quantum number $\kappa = \pm(j+1/2)$ for $l = j \pm 1/2$. \hat{A} denotes the antisymmetric operator to consider the exchange effect between the target electrons and the continuum electron. θ_q^{N+1} is a correlation function of the $(N+1)$ -electron system constructed based on a set of square-integrable orbitals to include additional correlation effects that are not sufficiently incorporated due to a cutoff in the sums over i and j , which is required to make the orbital wavefunctions orthogonalized and complete. The boundary between the internal and external regions is chosen in such a way that the magnitude of the radial spinor of the bound electrons is negligibly tiny at the boundary and the exchange effect between the bound and the continuum electrons outside the R-matrix

sphere is negligible. Both c_{ijk} and d_{qk} represent the corresponding expansion coefficients, which are determined by diagonalizing the Dirac Hamiltonian matrix of the $(N+1)$ -electron system. In addition, here i indicates the channel index, j the continuum basis function index, and k the eigenvector index.

The basis function $|\varepsilon \kappa m\rangle$ of continuum orbitals is approximated by a single-particle wavefunction as

$$|\varepsilon \kappa m\rangle = \frac{1}{r} \begin{pmatrix} P_{\varepsilon \kappa}(r) & \chi_{\kappa m}(\theta, \varphi) \\ iQ_{\varepsilon \kappa}(r) & \chi_{-\kappa m}(\theta, \varphi) \end{pmatrix}. \quad (3)$$

Here, $P(r)$ and $Q(r)$ are the (so-called) large and small components of the radial wave functions, respectively, and $\chi_{\kappa m}$ is the spin-angular functions.

With the wavefunctions of the $(N+1)$ -electron system and of the N -electron target ready, they can be used to obtain total photoionization cross section, which is given within the electric-dipole (E1) approximation as⁵²

$$\sigma = \frac{8\pi^2 \alpha C}{3(2J_i + 1)} \sum_{ij} |\langle \Psi_{j\kappa}^- || D_1 || \Psi_i \rangle|^2, \quad (4)$$

where the minus sign in the wavefunction $\Psi_{j\kappa}^-$ means that it has the asymptotic form of a Coulomb-modified plane wave in the final-state channel. D_1 represents the E1 transition operator of the radiation field

TABLE I. Energy levels (in units of Ryd) of W^{62+} ions compared with other available results. $\Delta\% = |MCDF - NIST|/NIST \times 100\%$.

Index	Configuration	$(^{2S+1}L_J)^\pi$	DARC	MCDF	RMBPT ⁶²	NIST ^{58–61}	$\Delta\%$
1	3s ²	$(^1S_0)^e$	0.00	0.00	0.00	0.00	
2	3s 3p	$(^3P_0)^o$	10.32	10.23	10.27	10.26 ^{60,61}	0.32
3		$(^3P_1)^o$	11.52	11.40	11.41	11.404 ⁵⁹	0.04
4	3p ²	$(^3P_0)^e$	24.80	25.05	24.49		
5	3s 3p	$(^3P_2)^o$	37.75	37.32	37.40	37.40 ^{60,61}	0.22
6		$(^1P_1)^o$	40.52	40.05	40.12	40.082 ⁵⁸	0.07
7	3p ²	$(^1D_2)^e$	50.97	50.72	50.44		
8		$(^3P_1)^e$	51.10	50.97	50.59		
9	3s 3d	$(^3D_1)^e$	53.66	53.14	53.10	53.10 ^{60,61}	0.08
10		$(^3D_2)^e$	54.69	54.35	54.04	54.042 ⁵⁸	0.56
11		$(^3D_3)^e$	59.97	59.41	59.21	59.21 ^{60,61}	0.33
12		$(^1D_2)^e$	61.28	60.61	60.49	60.49 ^{60,61}	0.20
13	3p 3d	$(^3F_2)^o$	64.84	64.61	64.16		
14		$(^3D_1)^o$	67.41	67.23	66.70		
15		$(^3P_2)^o$	72.49	72.13	71.67		
16		$(^3F_3)^o$	72.77	72.34	71.89		
17	3p ²	$(^3P_2)^e$	79.10	78.61	78.26		
18		$(^1S_0)^e$	80.66	80.23	79.66		
19	3p 3d	$(^3D_2)^o$	93.21	92.65	92.25		
20		$(^3P_0)^o$	93.90	93.40	92.99		
21		$(^3P_1)^o$	93.99	93.42	93.03		
22		$(^1F_3)^o$	94.01	93.44	92.99		
23		$(^3F_4)^o$	98.64	97.88	97.54		
24		$(^1D_2)^o$	99.49	98.37	98.40		
25		$(^3D_3)^o$	100.92	99.80	99.77		
26		$(^1P_1)^o$	101.82	100.76	100.70		

of ionizing light. α is the fine-structure constant. $C = \omega$ in the length gauge, while $C = 1/\omega$ in the velocity gauge. Note that in the photoionization process, non-dipole effects have been well known to be tiny from the infrared to the soft x-ray domains.^{54–56}

In the present work, all calculations are performed within the E1 approximation. The GRASP2K package on the basis of the MCDF method⁵⁷ is used to calculate all the desired bound-state wavefunctions and energy levels of W^{62+} ions. In order to acquire accurate atomic data for further calculations, 16 relativistic orbitals ($1s_{1/2}$, $2s_{1/2}$, $2p_{1/2}$, $2p_{3/2}$, $3s_{1/2}$, $3p_{1/2}$, $3p_{3/2}$, $3d_{3/2}$, $3d_{5/2}$, $4s_{1/2}$, $4p_{1/2}$, $4p_{3/2}$, $4d_{3/2}$, $4d_{5/2}$, $4f_{5/2}$, and $4f_{7/2}$) and 8 configurations ($1s^2 2s^2 2p^6 3s^2$, $1s^2 2s^2 2p^6 3s 3p$, $1s^2 2s^2 2p^6 3s 3d$, $1s^2 2s^2 2p^6 3p^2$, and $1s^2 2s^2 2p^6 3s 4l$ with $l = s, p, d, f$) are used, which results in 40 fine-structure energy levels. As performed in our previous work,⁵⁰ the obtained orbital wavefunctions are then used in the DSTG0 module of the DARC to produce the formatted file “TARGET.INP” which is required by the modules DSTG1 and DSTG2 for calculating the continuum orbitals and Hamiltonians, the radial and angular integrals, and the E1 matrix elements of the photoionization. Then, the associated Hamiltonian matrix is diagonalized in the module DSTGH and the photoionization cross sections are finally calculated with the use of the module PDSTG3. To obtain accurate wave functions and energy levels, the configurations chosen in the calculation of module DSTG2 are the same as those used in the GRASP2K package for the calculation of wave functions and energy levels. The boundary radius of the R-matrix sphere is taken to be $r = 1.15 a.u.$, which is sufficient to have all orbitals with $n \leq 4$ of W^{62+} ions incorporated and hence can guarantee that the orbital wavefunctions are complete in the R-matrix. In the calculation of resonant photoionization cross sections of W^{61+} ions we adopt 10^6 energy grid points with a step of 10^{-4} Ryd in order to find as many channels as possible. Of course, a small energy step and the resulting subtle cross sections can provide better understanding of the resonance structure associated with (narrow) innershell excitation channels.⁵³ For the resonant photoionization from the ground state $1s^2 2s^2 2p^6 3s^2 3p (J_i)^\pi = (1/2)^o$ of W^{61+} ions (channels = 73, Hamiltonian size = 2256), there are two possibilities allowed for the corresponding intermediate resonant states after photoexcitation, that is, $(J)^\pi = (1/2)^e$ (channels = 73, Hamiltonian size = 2258) and $(J)^\pi = (3/2)^e$ (channels = 128, Hamiltonian size = 3945).

III. RESULTS AND DISCUSSION

In Table I, we tabulate the presently calculated energy levels of W^{62+} ions associated with the configurations considered with the use of the DARC and GRASP2K packages. The present results are marked by DARC and MCDF, respectively, and compared with other results available from Refs. 58–62. Note that these energy levels are arranged energetically from low to high and that the ground-state energy level $1s^2 2s^2 2p^6 3s^2 ({}^1S_0)^e$ is set to be zero as a reference. As is clearly shown, the present DARC energy levels are slightly higher than the MCDF levels. This is because only the relativistic effect is incorporated into the DARC calculations but other contributions from the Breit interaction, the quantum-electrodynamical, and finite-nuclear-size effects are not taken into account.⁵² It is found that the present MCDF energy levels agree excellently with the RMBPT results of Kanti *et al.*⁶² and also with the NIST data.^{58–61} The maximum discrepancies are found to be less than 2.25% and 0.56%, respectively. Moreover, the present DARC

energy levels are also compared with the NIST results and a maximum discrepancy 1.31% is obtained. The excellent agreements obtained guarantee that the present energy levels and wavefunctions of W^{62+} ions further used to calculate the photoionization cross sections are reliable.

Figure 1 shows the cross sections of direct and resonant photoionization processes of W^{61+} ions from their ground state $[Mg]3p^2 P_{1/2}$ to all possible channels with $(J)^\pi = (1/2)^e$ and $(3/2)^e$, as functions of photoionizing energy. To further explain the reliability of the present calculations, the obtained results are presented for both the length and velocity gauges. The total photoionization cross sections are obtained by summing over the partial ones corresponding to the two types of channels with $(J)^\pi = (1/2)^e$ and $(3/2)^e$. As seen from the figure, the (total) photoionization cross sections obtained under the two gauges agree well with each other. Moreover, by comparison with the direct photoionization cross sections of Trzhaskovskaya and Nikulin,⁴⁸ a good agreement of the present results is also obtained, as can be seen from Table II for several photoionizing energies selected arbitrarily. In addition, it is found that the partial cross sections for the channels with $(J)^\pi = (3/2)^e$ are larger than those for the channels with $(J)^\pi = (1/2)^e$. Owing to the gauge consistency obtained, below we shall take only the results within the length gauge, for example, for further discussions.

In order to find direct and resonant photoionization limits and identify possible resonance channels of W^{61+} ions, the total photoionization cross sections within the length gauge are plotted solely in

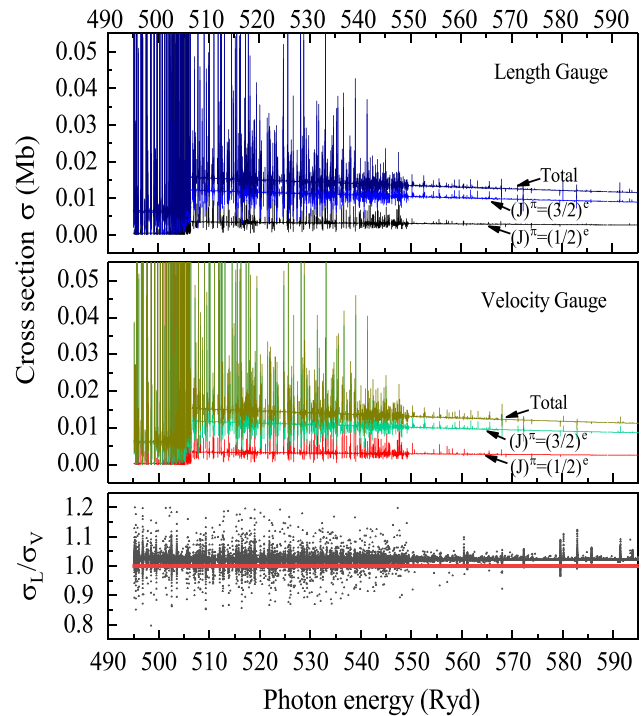
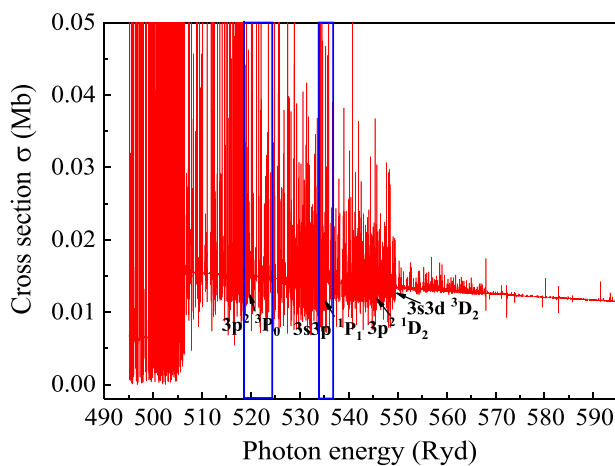


FIG. 1. Partial and total photoionization cross sections for direct and resonant photoionization of W^{61+} ions from their ground state $[Mg]3p^2 ({}^2P_{1/2})^o$. Results are presented for the length (top panel) and velocity (middle) gauges, along with the ratio σ_L/σ_V (bottom) of the total cross sections for both gauges.

TABLE II. Comparison of the present direct photoionization cross sections ($\times 10^{-3}$ Mb) with the results of Trzhaskovskaya and Nikulin⁴⁸ for several photoionizing energies (Ryd).

Index	Level	Photon energy (Ryd)	Reference ⁴⁸	Present	Discrepancy (%)
1	$^2P_{1/2}$	495.2008	6.478 877	6.479 895	0.016
2		498.0443	6.399 094	6.395 748	0.052
3		499.2103	6.366 775	6.363 634	0.049
4		503.1703	6.258 697	6.261 990	0.053
5		504.0098	6.236 115	6.233 637	0.040
6	$^2P_{3/2}$	468.1759	6.892 788	6.896 974	0.061
7		470.3169	6.818 801	6.817 968	0.012
8		474.2249	6.686 539	6.688 221	0.025
9		477.0009	6.594 722	6.595 365	0.010
10		482.5269	6.417 035	6.416 171	0.013

Fig. 2. It is found that the ionization limit of the direct photoionization of W^{61+} ions is 495.07 Ryd, which has a difference of 0.01% from the NIST result of 495.00 Ryd.⁶³ Such a difference results again from an incomplete inclusion of high-order corrections in the R-matrix method but hardly affects the photoionization cross sections. In addition to the direct ionization limit, several ionization limits of the resonant photoionization of W^{61+} ions are found as well. To be specific, the sudden changes in the continuous background of the photoionization cross sections indicate different resonant ionization limits, which correspond to the convergence of a particular Rydberg series. Take the obtained resonant ionization limit 519.87 Ryd for example, it is related to the convergence of the Rydberg series corresponding to the energy level $3p^2\ ^3P_0$, which is determined by the direct ionization limit 495.07 Ryd plus the excitation energy 24.80 Ryd of the level $3p^2\ ^3P_0$. The convergence limit of the Rydberg series at the energy point 505.39 Ryd is the ionization limit for the $1s^22s^22p^63s\ 3p\ (J_i)^\pi = (0)^o$ level of W^{62+} ions. This is because the Rydberg line system limit is where one successive electron of W^{61+} ions is at a very high principal quantum number, at which point the electron is just at infinity.

**FIG. 2.** Total photoionization cross sections for direct and resonant photoionization of W^{61+} ions from their ground state $[Mg]3p\ (^2P_{1/2})^o$. Results are presented only for the length gauge.

Therefore, when labeling the Rydberg line system limit, the energy level of W^{62+} ions is used. The Rydberg series convergence limit at the energy of 506.59 Ryd is the $1s^22s^22p^63s\ 3p\ (J_i)^\pi = (1)^o$ level of W^{62+} ions, which is the convergence of two different series of Rydberg states. There are also seven Rydberg series convergence limits for the photoionization in the energy range of 507–550 Ryd, which are listed in Table III together with the corresponding energy levels.

Apart from the photoionization limits, we also identify dominant resonant photoionization channels by elaborate analysis of the obtained energy levels of W^{61+} ions. These resonant photoionization channels are found to be associated with the resonances $3s3lnl'$ and $3p3lnl'$ ($l, l' = p, d$), which are listed explicitly as follows:

$$\begin{aligned}
 &W^{61+} [3s^23p^2P_{1/2}]_{1/2}^o + h\nu \\
 &\rightarrow W^{61+} [3s^2\ ^1S_0 + e^-(s, d)]_{1/2,3/2}^e \\
 &\rightarrow W^{61+} [3s3p\ ^1P_1 + e^-(p, f)]_{1/2,3/2}^e \\
 &\rightarrow W^{61+} [3s3p\ ^3P_{0,1,2} + e^-(p, f)]_{1/2,3/2}^e \\
 &\rightarrow W^{61+} [3p^2\ ^1S_0 + e^-(s, d)]_{1/2,3/2}^e \\
 &\rightarrow W^{61+} [3p^2\ ^1D_2 + e^-(s, d, h)]_{1/2,3/2}^e \\
 &\rightarrow W^{61+} [3p^2\ ^3P_{0,1,2} + e^-(s, d, h)]_{1/2,3/2}^e \\
 &\rightarrow W^{61+} [3s3d\ ^1D_2 + e^-(s, d, h)]_{1/2,3/2}^e \\
 &\rightarrow W^{61+} [3s3d\ ^3D_{1,2,3} + e^-(s, d, h)]_{1/2,3/2}^e \\
 &\rightarrow W^{61+} [3p3d\ ^1P_1 + e^-(p, f)]_{1/2,3/2}^e \\
 &\rightarrow W^{61+} [3p3d\ ^1D_2 + e^-(p, f)]_{1/2,3/2}^e \\
 &\rightarrow W^{61+} [3p3d\ ^1F_3 + e^-(p, f, i)]_{1/2,3/2}^e \\
 &\rightarrow W^{61+} [3p3d\ ^3P_{0,1,2} + e^-(p, f)]_{1/2,3/2}^e \\
 &\rightarrow W^{61+} [3p3d\ ^3D_{1,2,3} + e^-(p, f, i)]_{1/2,3/2}^e \\
 &\rightarrow W^{61+} [3p3d\ ^3F_{2,3,4} + e^-(p, f, i)]_{1/2,3/2}^e
 \end{aligned}$$

It is found that the obtained resonance peaks corresponding to an identical or various different Rydberg series are densely spaced in the photon energy range 495–570 Ryd. These resonance peaks overlap partially or even fully with each other and are hardly distinguishable. Actually, this kind of resonance peaks is very narrow and the corresponding Rydberg resonance series converges quickly to its excitation threshold.⁶⁴ From a theoretical point of view, the overlap of these

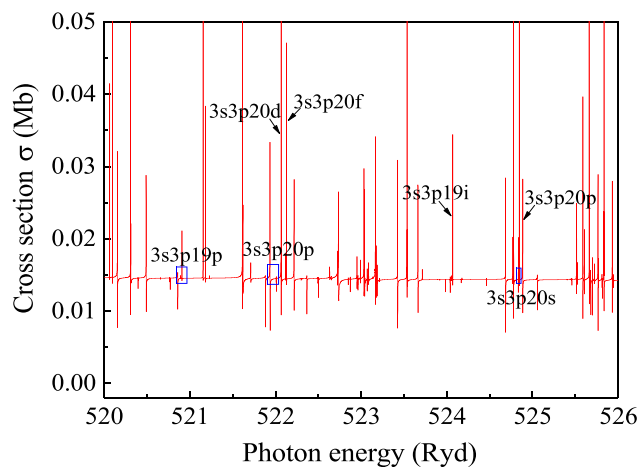
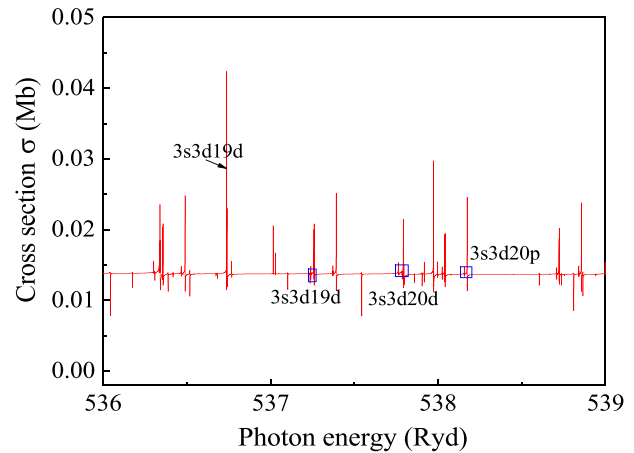
TABLE III. Ionization limits for the resonant photoionization processes of W^{61+} ions from their ground state.

Index	Level	Energy (Ryd)
1	$3p^2\ ^3P_0$	519.87
2	$3s3p\ ^3P_2$	532.82
3	$3s3p\ ^1P_1$	535.59
4	$3p^2\ ^1D_2$	546.04
5	$3p^2\ ^3P_1$	546.17
6	$3s3d\ ^3D_1$	548.73
7	$3s3d\ ^3D_2$	549.76

resonance peaks is caused by a relativistic intermixing and coupling of the channels listed above.³⁴ It is also found that the resonance peaks beyond the energy of 570 Ryd become extremely weak and, hence, further calculations for higher photon energies are not performed in the present work.

As the obtained resonance peaks are densely spaced and thus are hardly identified, we select two areas with relatively sparse peaks in the energy ranges 520–526 and 536–539 Ryd (i.e., the areas in the blue boxes of Fig. 2) to identify more specifically the corresponding resonant photoionization channels, as shown in Figs. 3 and 4, respectively. By detailed analysis of the energy levels of the obtained W^{61+} ions and comparison with the positions of these peaks, eight and six relatively isolated resonance peaks are identified at a fine-structural or configurational level for the two areas, respectively, as labeled in Figs. 3 and 4 as well as listed in Tables IV and V, respectively. For example, the resonance peak at the photon energy of 520.86 Ryd is identified to be associated with the fine-structure energy level $3s3p19p\ (J)^\pi = (3/2)^e$. Nevertheless, the resonance peaks in other areas are densely spaced and hence indistinguishable even at a configurational level.

In addition to the photoionization of W^{61+} ions from their ground state $[Mg]3p\ ^2P_{1/2}$, the direct and resonant photoionization of W^{61+} ions from four lowly excited states (i.e. $[Ne]3s3p^2\ ^4P_{1/2,3/2}$, $[Mg]3p^2\ ^3P_{3/2}$, and $[Ne]3s3p^2\ ^2D_{5/2}$) are also studied. The obtained total cross sections in the length gauge are plotted in Fig. 5. Overall,

**FIG. 3.** The same as Fig. 2 but for the energy range 520–526 Ryd.**FIG. 4.** The same as Fig. 2 but for the energy range 536–539 Ryd.

very similar results to the case of the ground-state photoionization are obtained for the photoionization of W^{61+} ions from the four lowly excited states. The direct photoionization limits 456.49, 457.90, 468.07, and 482.64 Ryd are obtained for the excited states $^2D_{5/2}$, $^4P_{3/2}$, $^2P_{3/2}$, and $^4P_{1/2}$, respectively, which have discrepancies of 0.09%, 0.07%, 0.04%, and 0.01% in contrast to the NIST data 456.89,^{60,61} 458.23,⁵⁸ 468.27,⁵⁹ and 482.69 Ryd,⁵⁹ respectively. Once again, these small discrepancies result from an incomplete inclusion of high-order corrections in the R-matrix method, which hardly affect the reliability and accuracy of the presently obtained photoionization cross sections. As for the resonant photoionization limits and resonance peaks for these excited states, they are hardly distinguishable and thus are not presented in the present work due to much more densely spaced resonance peaks and more complicated resonance structures than the case of the ground-state photoionization. We expect that the present photoionization data of W^{61+} ions could be helpful to the diagnosis and simulation of the thermonuclear fusion plasmas together with other available photoionization data of tungsten ions with various charge states.

IV. SUMMARY

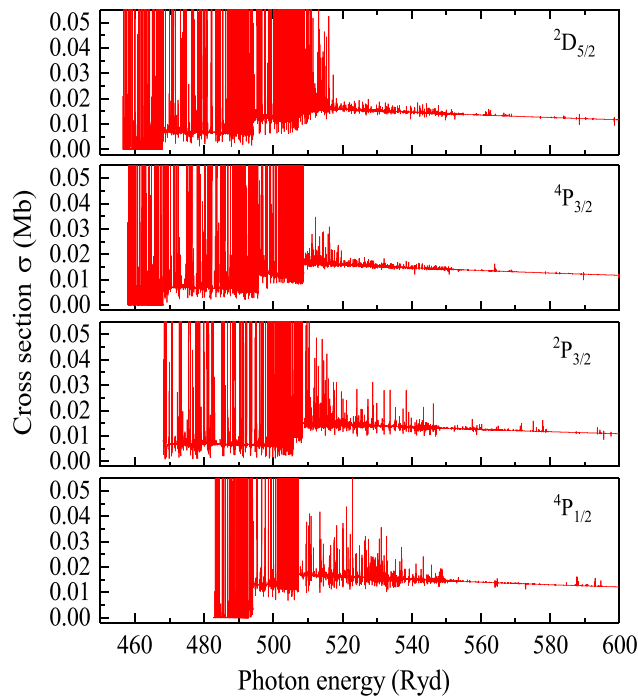
To be summarized, the direct and resonant photoionization of W^{61+} ions from their ground state $[Mg]3p\ ^2P_{1/2}$ as well as four lowly

TABLE IV. The energies corresponding to the resonance peaks of the ground state $^2P_{1/2}$ of W^{61+} ions in the energy range 520–526 Ryd.

Index	Level	Energy (Ryd)
1	$3s3p19p\ (J)^\pi = (3/2)^e$	520.86
2	$3s3p20p\ (J)^\pi = (5/2)^e$	521.93
3	$3s3p20p\ (J)^\pi = (1/2)^e$	522.02
4	$3s3p20d\ (J)^\pi = (9/2)^o$	522.07
5	$3s3p20f\ (J)^\pi = (3/2)^e$	522.12
6	$3s3p19i\ (J)^\pi = (11/2)^o$	524.06
7	$3s3p20s\ (J)^\pi = (3/2)^o$	524.84
8	$3s3p20p\ (J)^\pi = (3/2)^e$	524.88

TABLE V. The same as Table IV but for the energy range 536–539 Ryd.

Index	Level	Energy (Ryd)
1	$3s3p19d (J)^\pi = (1/2)^o$	536.73
2	$3s3p19d (J)^\pi = (5/2)^o$	537.24
3	$3s3p19d (J)^\pi = (3/2)^o$	537.26
4	$3s3p20d (J)^\pi = (5/2)^o$	537.78
5	$3s3p20d (J)^\pi = (7/2)^o$	537.81
6	$3s3d20p (J)^\pi = (5/2)^o$	538.17

**FIG. 5.** The same as Fig. 2 but for the photoionization of W^{61+} ions from the excited states $[Ne]3s3p^2 4P_{1/2}$, $[Ne]3s^2 3p^2 P_{3/2}$, $[Ne]3s 3p^2 4P_{3/2}$, and $[Ne]3s 3p^2 2D_{5/2}$.

excited states $[Ne]3s3p^2 4P_{1/2,3/2}$, $[Mg]3p^2 P_{3/2}$, and $[Ne]3s3p^2 2D_{5/2}$ is studied by using the relativistic R-matrix method and the MCDF method. All the required wavefunctions and energy levels are produced from the GRASP2K package. Good agreements with other available energy-level results are obtained. With the use of the obtained MCDF wavefunctions, the photoionization cross sections are calculated by means of the DARCF package. For the ground-state photoionization, we obtain the direct and resonant photoionization limits and identify part of resonance peaks at the level of fine-structure energy levels or configurations. The identified resonance peaks are found to be associated with the resonances $3s3lnl'$ and $3p3lnl'$ ($l, l' = p, d$). For the excited-state photoionization, however, the corresponding resonant ionization limits and resonance peaks are hardly distinguishable due to much more densely spaced resonance peaks and more complicated resonance structure than the case of the ground-state photoionization, although the respective direct photoionization limits are obtained. It is

expected that the present work could fill the existing vacancy of studies on the photoionization of W^{61+} ions and be helpful to the diagnosis and simulation of the thermonuclear fusion plasmas together with available photoionization data of tungsten ions with other charge states.

ACKNOWLEDGMENTS

This work was funded by the National Natural Science Foundation of China under Grants Nos. 12174315 and 11804280, the Chinese Scholarship Council under Grant No. 202008620004, the Outstanding Youth Fund of the Science and Technology Project of Gansu Province under Grant No. 23JRRA687, and the Youth Science and Technology Talent Promotion Project of Gansu Province under Grant No. GXH2020626-09.

AUTHOR DECLARATIONS

Conflict of Interest

The authors have no conflicts to disclose.

Author Contributions

Z. W. Wu: Conceptualization (lead); Data curation (equal); Funding acquisition (lead); Writing – original draft (equal). **J. Q. Wang:** Data curation (equal); Formal analysis (lead); Writing – original draft (equal); Writing – review & editing (lead). **Y. Li:** Formal analysis (supporting); Writing – review & editing (supporting). **Y. H. An:** Formal analysis (supporting). **S. Fritzsche:** Supervision (lead); Writing – review & editing (supporting).

DATA AVAILABILITY

The data that support the findings of this study are available from the corresponding author upon reasonable request.

REFERENCES

- J. M. Bizau, J. M. Esteve, D. Cubaynes, F. J. Wuilleumier, C. Blancard, A. C. La Fontaine, C. Couillaud, J. Lachkar, R. Marmoret, C. Rémond, J. Bruneau, D. Hitz, P. Ludwig, and M. Delaunay, "Photoionization of highly charged ions using an ECR ion source and undulator radiation," *Phys. Rev. Lett.* **84**, 435 (2000).
- A. Müller, A. Borovik, T. Buhr, J. Hellhund, K. Holste, A. L. D. Kilcoyne, S. Klumpp, M. Martins, S. Ricz, J. Viehhaus, and S. Schippers, "Observation of a four-electron auger process in near-k-edge photoionization of singly charged carbon ions," *Phys. Rev. Lett.* **114**, 013002 (2015).
- A. Müller, E. Lindroth, S. Bari, A. Borovik, P. M. Hillenbrand, K. Holste, P. Indelicato, A. L. D. Kilcoyne, S. Klumpp, M. Martins, J. Viehhaus, P. Wilhelm, and S. Schippers, "Photoionization of metastable heliumlike C^{4+} ($1s2s^3S_1$) ions: Precision study of intermediate doubly excited states," *Phys. Rev. A* **98**, 033416 (2018).
- F.-I. Wang, S. Fujioka, H. Nishimura, D. Kato, Y.-t. Li, G. Zhao, J. Zhang, and H. Takabe, "Experimental evidence and theoretical analysis of photoionized plasma under x-ray radiation produced by an intense laser," *Phys. Plasmas* **15**, 073108 (2008).
- B. A. Remington, R. P. Drake, and D. D. Ryutov, "Experimental astrophysics with high power lasers and z pinches," *Rev. Mod. Phys.* **78**, 755–807 (2006).
- F. Paerels, J. Cottam, M. Sako, D. A. Liedahl, A. Brinkman, R. Van der Meer, J. Kaastra, and P. Predehl, "High-resolution spectroscopy of the x-ray-photoionized wind in Cygnus x-3 with the Chandra high-energy transmission grating spectrometer," *Astrophys. J.* **533**, L135 (2000).
- D. Lai and W. C. Ho, "Polarized x-ray emission from magnetized neutron stars: Signature of strong-field vacuum polarization," *Phys. Rev. Lett.* **91**, 071101 (2003).

- ⁸J. D. Schnittman and J. H. Krolik, "X-ray polarization from accreting black holes: The thermal state," *Astrophys. J.* **701**, 1175 (2009).
- ⁹A. Müller, S. Schippers, R. A. Phaneuf, A. L. D. Kilcoyne, H. Bräuning, A. S. Schlachter, M. Lu, and B. M. McLaughlin, "Fine-structure resolved photoionization of metastable Be-like ions C III, N IV, and O V," *J. Phys. Conf. Ser.* **58**, 383 (2007).
- ¹⁰A. Singh, D. Dawra, M. Dimri, A. K. Jha, R. Sharma, and M. Mohan, "Relativistic photoionization cross section calculations and resonance parameters for Mg-like Se XXIII," *Rad. Phys. Chem.* **168**, 108447 (2020).
- ¹¹E. Kennedy, J.-P. Mosnier, P. Van Kampen, D. Cubaynes, S. Guibaud, C. Blancard, B. McLaughlin, and J.-M. Bizau, "Photoionization cross sections of the aluminumlike Si⁺ ion in the region of the 2p threshold (94–137 eV)," *Phys. Rev. A* **90**, 063409 (2014).
- ¹²R. Nazir, M. Bari, S. Sardar, M. Bilal, M. Salahuddin, and M. Nasim, "Dirac R-matrix calculations of photoionization cross-sections of Ca IV," *Mon. Not. R. Astron. Soc.* **462**, 3703–3709 (2016).
- ¹³A. K. Singh, D. Dawra, M. Dimri, A. K. Jha, and M. Mohan, "Relativistic r-matrix calculations of photoionization cross sections of Cu XVIII," *Eur. Phys. J. D* **73**, 85 (2019).
- ¹⁴L. Liang and C. Zhou, "K-shell photoionization of Be-like nitrogen from the ground state: Energies and Auger widths of the high-lying double-excited states for N IV," *Can. J. Phys.* **96**, 1183–1191 (2018).
- ¹⁵H. Wang and G. Jiang, "Theoretical photoionization study of Ti⁹⁺ ion," *Can. J. Phys.* **99**, 323–328 (2021).
- ¹⁶S. N. Nahar and A. K. Pradhan, "Electron-ion recombination in the close-coupling approximation," *Phys. Rev. Lett.* **68**, 1488–1491 (1992).
- ¹⁷C. Fischer, G. Tachiev, G. Gaigalas, and M. Godefroid, "An MCHF atomic-structure package for large-scale calculations," *Comput. Phys. Commun.* **176**, 559–579 (2007).
- ¹⁸Y. Yan and M. J. Seaton, "Atomic data for opacity calculations. IV. photoionisation cross sections for C II," *J. Phys. B: At. Mol. Opt. Phys.* **20**, 6409–6429 (1987).
- ¹⁹F. Parpia, C. Fischer, and I. Grant, "Grasp92: A package for large-scale relativistic atomic structure calculations," *Comput. Phys. Commun.* **94**, 249–271 (1996).
- ²⁰P. G. Burke and K. T. Taylor, "R-matrix theory of photoionization. Application to neon and argon," *J. Phys. B: At. Mol. Opt. Phys.* **8**, 2620–2639 (1975).
- ²¹A. Aguilar, J. D. Gillaspay, G. F. Gribakin, R. A. Phaneuf, M. F. Gharabeh, M. G. Kozlov, J. D. Bozek, and A. L. D. Kilcoyne, "Absolute photoionization cross sections for Xe⁴⁺, Xe⁵⁺, and Xe⁶⁺ near 13.5 nm: Experiment and theory," *Phys. Rev. A* **73**, 032717 (2006).
- ²²H. Kjeldsen, "Photoionization cross sections of atomic ions from merged-beam experiments," *J. Phys. B: At. Mol. Opt. Phys.* **39**, R325–R377 (2006).
- ²³M. C. Simon, M. Schwarz, S. W. Epp, C. Beilmann, B. L. Schmitt, Z. Harman, T. M. Baumann, P. H. Mokler, S. Bernitt, R. Ginzl, S. G. Higgins, C. H. Keitel, R. Klawitter, K. Kubiček, V. Mäkel, J. Ullrich, and J. R. C. López-Urrutia, "Photoionization of N³⁺ and Ar⁸⁺ in an electron beam ion trap by synchrotron radiation," *J. Phys. B: At. Mol. Opt. Phys.* **43**, 065003 (2010).
- ²⁴J. B. West, "Photoionization of atomic ions," *J. Phys. B: At. Mol. Opt. Phys.* **34**, R45–R91 (2001).
- ²⁵N. El Hassan, J. M. Bizau, C. Blancard, P. Cossé, D. Cubaynes, G. Faussurier, and F. Folkmann, "Photoionization cross sections of iron isonuclear sequence ions: Fe²⁺ to Fe⁶⁺," *Phys. Rev. A* **79**, 033415 (2009).
- ²⁶M. J. Seaton, "Atomic data for opacity calculations. I. General description," *J. Phys. B: At. Mol. Opt. Phys.* **20**, 6363–6378 (1987).
- ²⁷W. Cunto, C. Mendoza, F. Ochsenbein, and C. J. Zeippen, "TOPbase at the CDS," *Astron. Astrophys.* **275**, L5 (1993).
- ²⁸D. G. Hummer, K. A. Berrington, W. Eissner, A. K. Pradhan, H. E. Saraph, J. A. Tully, D. G. Hummer, K. A. Berrington, W. Eissner, and A. K. Pradhan, "Atomic data from the iron project. I: Goals and methods," *Astron. Astrophys.* **279**, 298–309 (1993).
- ²⁹X. B. Ding, R. Sun, J. X. Liu, F. Koike, I. Murakami, D. Kato, H. A. Sakaue, N. Nakamura, and C. Z. Dong, "E1, M1, E2 transition energies and probabilities of W⁵⁴⁺ ions," *J. Phys. B: At. Mol. Opt. Phys.* **50**, 045004 (2017).
- ³⁰X. B. Ding, J. X. Liu, F. Koike, I. Murakami, D. Kato, H. A. Sakaue, N. Nakamura, and C. Z. Dong, "Collisional-radiative model for the visible spectrum of W²⁶⁺ ions," *Phys. Lett. A* **380**, 874–877 (2016).
- ³¹X. B. Ding, R. Sun, F. Koike, I. Murakami, D. Kato, H. A. Sakaue, N. Nakamura, and C. Z. Dong, "Energy levels, lifetimes and radiative data of W LV," *At. Data Nucl. Data Tables* **119**, 354–425 (2018).
- ³²T. Pütterich, R. Neu, R. Dux, A. D. Whiteford, and M. G. O'Mullane, "Modelling of measured tungsten spectra from ASDEX Upgrade and predictions for ITER," *Plasma Phys. Controlled Fusion* **50**, 085016 (2008).
- ³³P. Beiersdorfer, J. Clementson, J. Dunn, M. F. Gu, K. Morris, Y. Podpaly, E. Wang, M. Bitter, R. Feder, K. W. Hill, D. Johnson, and R. Barnsley, "The ITER core imaging x-ray spectrometer," *J. Phys. B: At. Mol. Opt. Phys.* **43**, 144008 (2010).
- ³⁴I. Khatri, A. Goyal, S. Aggarwal, A. Singh, and M. Mohan, "R-matrix calculations of photoionization cross section of Ne-like tungsten," *Can. J. Phys.* **93**, 1221–1226 (2015).
- ³⁵J. J. Boyle, Z. Altun, and H. P. Kelly, "Photoionization cross-section calculation of atomic tungsten," *Phys. Rev. A* **47**, 4811–4830 (1993).
- ³⁶P. Sladeczek, M. Feist, M. Feldt, M. Martins, and P. Zimmermann, "Photoionization experiments with an atomic beam of tungsten in the region of the 5p and 4f excitation," *Phys. Rev. Lett.* **75**, 1483–1486 (1995).
- ³⁷C. P. Ballance and B. M. McLaughlin, "Photoionization of the valence shells of the neutral tungsten atom," *J. Phys. B: At. Mol. Opt. Phys.* **48**, 085201 (2015).
- ³⁸B. M. McLaughlin and C. P. Ballance, "Photoionization of the neutral tungsten atom," *J. Phys. Conf. Ser.* **635**, 092053 (2015).
- ³⁹A. Müller, S. Schippers, J. Hellhund, K. Holste, A. L. D. Kilcoyne, R. A. Phaneuf, C. P. Ballance, and B. M. McLaughlin, "Single-photon single ionization of W⁺ ions: Experiment and theory," *J. Phys. B: At. Mol. Opt. Phys.* **48**, 235203 (2015).
- ⁴⁰B. M. McLaughlin, C. P. Ballance, S. Schippers, J. Hellhund, A. L. D. Kilcoyne, R. A. Phaneuf, and A. Müller, "Photoionization of tungsten ions: Experiment and theory for W²⁺ and W³⁺," *J. Phys. B: At. Mol. Opt. Phys.* **49**, 065201 (2016).
- ⁴¹A. Müller, S. Schippers, J. Hellhund, A. L. D. Kilcoyne, R. A. Phaneuf, and B. M. McLaughlin, "Photoionization of tungsten ions: Experiment and theory for W⁴⁺," *J. Phys. B: At. Mol. Opt. Phys.* **50**, 085007 (2017).
- ⁴²A. Müller, S. Schippers, J. Hellhund, A. L. D. Kilcoyne, R. A. Phaneuf, and B. M. McLaughlin, "Photoionization of tungsten ions: Experiment and theory for W⁵⁺," *J. Phys. B: At. Mol. Opt. Phys.* **52**, 195005 (2019).
- ⁴³A. Müller, S. Schippers, A. L. D. Kilcoyne, and D. Esteves, "Photoionization of tungsten ions with synchrotron radiation," *Phys. Scr.* **T144**, 014052 (2011).
- ⁴⁴A. Müller, S. Schippers, J. Hellhund, A. L. D. Kilcoyne, R. A. Phaneuf, C. P. Ballance, and B. M. McLaughlin, "Single and multiple photoionization of W^{q+} tungsten ions in charge states q=1, 2,...,5: Experiment and theory," *J. Phys. Conf. Ser.* **488**, 022032 (2014).
- ⁴⁵M. Trzhaskovskaya, V. Nikulin, and Y. Tsarev, "Radiative recombination data for low-charged tungsten ions: IV. W³⁺–W¹³⁺," *At. Data Nucl. Data Tables* **139**, 101389 (2021).
- ⁴⁶M. Trzhaskovskaya and V. Nikulin, "Radiative recombination data for tungsten ions: III. W¹⁴⁺–W²³⁺," *At. Data Nucl. Data Tables* **100**, 1156–1188 (2014).
- ⁴⁷M. B. Trzhaskovskaya and V. K. Nikulin, "Radiative recombination data for tungsten ions: I. W²⁴⁺–W⁴⁵⁺," *At. Data Nucl. Data Tables* **99**, 249–311 (2013).
- ⁴⁸M. B. Trzhaskovskaya and V. K. Nikulin, "Radiative recombination data for tungsten ions: II. W⁴⁷⁺–W⁷¹⁺," *At. Data Nucl. Data Tables* **100**, 986–1058 (2014).
- ⁴⁹S. D. López, J. M. Randazzo, R. D. Picca, and F. D. Colavecchia, "W⁶³⁺ and W⁶⁴⁺ ionization by protons and photons," *J. Phys. Conf. Ser.* **583**, 012035 (2015).
- ⁵⁰Y. H. An, Z. W. Wu, J. Jiang, L. Y. Xie, D. H. Zhang, and C. Z. Dong, "Relativistic R-matrix calculations of the photoionization of W⁶³⁺ ions," *J. Phys. B: At. Mol. Opt. Phys.* **54**, 065001 (2021).
- ⁵¹E. P. Wigner and L. Eisenbud, "Higher angular momenta and long range interaction in resonance reactions," *Phys. Rev.* **72**, 29–41 (1947).
- ⁵²P. H. Norrington, "Dirac Atomic R-matrix Codes," (2004), <http://www.am.qub.ac.uk/DARC>.
- ⁵³S. Sardar, M. Bilal, R. Tariq Nazir, M. Bari, A. Hannan, and M. Nasim, "Dirac R-matrix calculations of photoionization cross sections of Fe XVI," *Mon. Not. R. Astron. Soc.* **450**, 1631–1637 (2015).
- ⁵⁴T. Liang, M. Han, Y. J. Liao, J. B. Ji, C. S. Leung, W. C. Jiang, K. Ueda, Y. M. Zhou, P. X. Lu, and H. J. Wörner, "Attosecond-resolved non-dipole photoionization dynamics," *Nat. Photonics* **18**, 311–317 (2024).

- ⁵⁵P. V. Demekhin, "On the breakdown of the electric dipole approximation for hard x-ray photoionization cross sections," *J. Phys. B: At. Mol. Opt. Phys.* **47**, 025602 (2014).
- ⁵⁶M. K. Inal, A. Surzhykov, and S. Fritzsche, "Linear polarization of the $2p^5 3s \rightarrow 2p^6$ lines following the inner-shell photoionization of sodiumlike ions," *Phys. Rev. A* **72**, 042720 (2005).
- ⁵⁷P. Jönsson, X. He, C. Froese Fischer, and I. P. Grant, "The grasp2K relativistic atomic structure package," *Comput. Phys. Commun.* **177**, 597–622 (2007).
- ⁵⁸J. Clementson and P. Beiersdorfer, "Wavelength measurement of $n = 3$ to $n = 3$ transitions in highly charged tungsten ions," *Phys. Rev. A* **81**, 052509 (2010).
- ⁵⁹Y. Ralchenko, I. Draganic, J. Tan, J. Gillaspay, J. Pomeroy, J. Reader, U. Feldman, and G. Holland, "EUV spectra of highly-charged ions W^{54+} – W^{63+} relevant to ITER diagnostics," *J. Phys. B: At. Mol. Opt. Phys.* **41**, 021003 (2008).
- ⁶⁰J. Clementson, P. Beiersdorfer, G. Brown, M. Gu, H. Lundberg, Y. Podpaly, and E. Träbert, "Tungsten spectroscopy at the Livermore electron beam ion trap facility," *Can. J. Phys.* **89**, 571–580 (2011).
- ⁶¹U. I. Safronova and A. S. Safronova, "Wavelengths and transition rates for $nl-n'l'$ transitions in Be-, B-, Mg-, Al-, Ca-, Zn-, Ag- and Yb-like tungsten ions," *J. Phys. B: At. Mol. Opt. Phys.* **43**, 074026 (2010).
- ⁶²K. M. Aggarwal and F. P. Keenan, "Radiative rates for E1, E2, M1, and M2 transitions in S-like to F-like tungsten ions (WLIX to WLXVI)," *At. Data Nucl. Data Tables* **111–112**, 187–279 (2016).
- ⁶³A. E. Kramida and J. Reader, "Ionization energies of tungsten ions: W^{2+} through W^{71+} ," *At. Data Nucl. Data Tables* **92**, 457–479 (2006).
- ⁶⁴A. K. Singh, M. Dimri, D. Dawra, A. K. S. Jha, and M. Mohan, "Relativistic R-matrix photoionization cross section calculations of Ne-like CoXVIII with resonance parameters," *J. Phys. B: At. Mol. Opt. Phys.* **52**, 075002 (2019).